VEHICLE SYSTEM DYNAMICS
https://doi.org/10.1080/00423114.2024.2361726

Path-tracking control at the limits of handling of a prototype over-actuated autonomous vehicle

Chenhui Lin, Efstathios Siampis and Efstathios Velenis

Advanced Vehicle Dynamics Centre, Cranfield University, Cranfield, UK

ABSTRACT

Considering the vehicle dynamics at the limits of handling is vital to improve the performance and safety of autonomous vehicles especially in extreme situations. This paper presents the development of a path-tracking controller for an over-actuated autonomous vehicle. The vehicle is an electric prototype equipped with torque vectoring and four-wheel steering, which enable enhanced control of vehicle dynamics. A model predictive controller is proposed taking into account the nonlinearities in vehicle dynamics at the limits of handling as well as the crucial actuator constraints. The controller is examined in both high-fidelity simulation and practical testing to validate the vehicle's handling performance. Both the simulation and testing results illustrate that the over-actuation topology can enhance the handling performance as well as vehicle stability at conditions close to the limits of handling. With additional references such as side slip angle, the vehicle's attitude under such extreme condition can also be manipulated. The testing also demonstrates the real-time capability of the controller. Further testing has been done to confirm that side slip angle reference plays an important role in path-tracking control at the limits of handling, and to push the vehicle to the friction limits.

ARTICLE HISTORY
Received 6 December 2023
Revised 22 April 2024
Accepted 24 May 2024

KEYWORDS
Autonomous vehicle; multi-actuation; predictive control; path-tracking

1. Introduction

Over the past few decades, due to the increasing demands to improve the safety, efficiency and comfort of road vehicles, autonomous vehicles (AVs) have been widely considered as the next generation of road transportation. The control techniques for AVs have been rapidly developed with a great deal of research work carried out for various objectives, including path and motion planning [1–3], path-tracking [4,5], obstacle detection and avoidance [6,7] and so forth. Among these topics, path-tracking as one of the fundamental functions of AVs, and the real-time realisation of it, is the main focus of this paper.

Regarding the path-tracking problem, geometry-based control methods have been raised for active front-wheel steering (FWS) vehicles [8,9]. Geometric path-tracking controllers are able to track a path only with the geometry of vehicle kinematics and of the reference path, but they are less suitable for control at the limits of handling due to the lack

CONTACT Chenhui Lin chenhui.lin@cranfield.ac.uk

of consideration on vehicle dynamics. In terms of the path-tracking controllers involving vehicle dynamics, Roselli et al. proposed a path-tracking controller for lane-keeping based on the H-infinity technique [10]. According to the experimental tests, the H-infinity controller was able to achieve overall smaller lateral error in comparison with a PID controller with feedforward, and thus a smoother action in the corner was achieved. In another study, a higher-order sliding mode controller was designed for lateral control, and robustness was validated by the test results [11]. In addition to these, optimal control theory has also been introduced to the scope. Lee et al. proposed an optimal path-tracking controller based on linear quadratic Gaussian control, which provided better performance than the geometry-based controllers in terms of tracking deviation [12]. However, path-tracking was not carried out close to the vehicles' handling limit in these work.

Among various control methods, model predictive control (MPC) has been found as an outstanding technique for autonomous vehicle control. In Ref. [13], geometric controller, linear quadratic regulator and MPC were compared, and it was demonstrated in simulation that the best path-tracking performance was achieved by MPC with the minimum control effort. Yakub et al. extended the study by comparing the tracking performance of MPC and linear quadratic control for different speed, tyre-road friction coefficients and control topologies, including FWS, four-wheel steering (4WS) and FWS with direct yaw moment control (DYC) [14]. Despite the vehicle not operating at the limits of handling in this work, a similar conclusion was drawn that MPC was more suitable for multi-variable systems. In addition to that, the advantage of MPC has also been demonstrated with regard to the inclusion of constraints due to the presence of state ranges, input limitations and road boundaries. Therefore, MPC has been broadly applied in the academia for the purpose of path-tracking control [15–18]. In Ref. [18], Awad et al. developed a path-tracking control algorithm with a fuzzy logic switching system, and the proposed controller was able to track the reference path in relatively low speed condition. In Ref. [17], a path-tracking controller with an adaptive preview strategy was developed, while the simulation results showed that the tracking error significantly increased when the vehicle got close to the ground-tyre adhesion limit. In the above studies, linear models or linearised models are used to represent vehicle dynamics. This would help to reduce the complexity of the MPC problem. However, in the situation such as operation at the limits of handling or where multi-actuation is applied, the vehicle behaviour becomes highly nonlinear and in such case, the linear model may no longer be sufficient to guarantee good prediction of the vehicle dynamics.

In addition to active FWS control, techniques like DYC, torque vectoring (TV) in particular, has been extensively discussed in the literature for vehicle control. Typically, TV refers to the technique which varies the torque delivered on each wheel. With the development of electric vehicles (EVs), the application of independent in-wheel motors provides a more straightforward realisation of TV. In Ref. [19], several path-tracking controllers with TV were compared with some other controllers without the functionality, and it was showed that the cornering response could be effectively improved at the limits of handling by TV control, where the generation of a direct yaw moment benefited stabilisation of the vehicle. Hence, TV has been applied in many studies on driver assist system development, aiming to improve vehicle performance and achieve consistently safe and stable cornering response [20–22]. There is no doubt that AV control can benefit from the multi-actuation formulation, referring to the integration of TV and steering. Guo et al.

developed a path-tracking controller with real-time implementability, in which MPC was applied based on an LTV system [23]. The controller had a hierarchical structure, where the required steering angle and yaw moment were identified at the higher level, and those requirements were then achieved through control allocation at the lower level. In Ref. [24], a path-tracking controller was proposed for the vehicles with four-wheel drive (4WD) as well as 4WS. This controller also had a hierarchical structure, and applied linear vehicle and tyre models. Such formulation excluded steering from the control allocation strategy, which could lead to suboptimality in the results. What's more, because of the linear systems applied in the higher level controllers, performance as well as feasibility could hardly be guaranteed, especially in extreme conditions. This could hinder the vehicle from operating at the limits of handling. In Ref. [25], Acosta et al. proposed a multi-actuation controller for autonomous drift control based on nonlinear vehicle and tyre models, and it showed that the combination of FWS and TV can potentially exploit the vehicle's dynamical capability. However, this work applied a PID controller for path-tracking instead of including it in the MPC strategy, which meant that the vehicle might not be able to follow complex path properly. In addition, the controller was not experimentally validated.

In the literature, significant amount of work has been carried out on the topic of path-tracking control of autonomous vehicles, while path-tracking at the limits of handling, over-actuation control and real-time control implementation have rarely been achieved on a full-size vehicle at the same time. Kapania and Gerdes [26], Torres et al. [27] have presented work on real-time path-tracking control at the limits of handling, while they were based on less actuation and more simplified vehicle dynamics models are applied. Barari et al. [28] worked on path-tracking control of a multi-actuated vehicle with potential real-time capability, while the operation was not close to the limits of handling. Hiraoka et al. [29], Ren et al. [30], Jeong and Yim [31] have developed control strategies for path-tracking with multi-actuation systems, but these work has not been implemented or validated in real time. The key contribution of this work is addressing all the three aspects simultaneously.

In this paper, we present the development of a path-tracking controller for an over-actuated autonomous EV, which is equipped with 4WS as well as TV capability at the rear axle. The vehicle is tasked to follow a desired path at specified reference velocity, such that the vehicle operates at its handling limit that is at the limit of the tyres' adhesion. The control design is based on nonlinear MPC (NMPC) so that the nonlinearities of the vehicle dynamics is taken into account, which is beneficial to the operation at the limits of handling. The developed controller is validated in both simulation and testing, and shows the advantage of the over-actuation topology in enhancing the vehicle's stability and performance at the limits of handling. In addition, it is also demonstrated that with additional state reference such as side slip angle, the vehicle's attitude can also be manipulated under extreme conditions. The implementation of the NMPC control framework for multi-actuated vehicle path-tracking control on an experimental vehicle platform has been introduced in Ref. [32]. Further to the discussion in Ref. [32], this paper presents the detailed formulation of the controller together with a focused and systematic analysis of the controller's performance in limits handling conditions, including the effect of side slip angle reference tracking. The major contribution of this paper can be summarised as three parts. First, this paper proposes a control formulation based on NMPC which is compatible with an over-actuation topology, and the results demonstrate that the over-actuation

formulation is able to enhance path-tracking performance for autonomous vehicle at the limits of handling. Secondly, it is demonstrated that the proposed controller including the particular over-actuation formulation as well as nonlinear vehicle dynamics can be implemented in real time, and the proposed controller has been implemented on a full-size test vehicle and validated in practice. Appropriate prediction horizon and sampling time have been determined for the controller, which strike a balance between path-tracking performance and system complexity. Last but not least, the effect of side slip angle reference in the control performance of path-tracking at the limits of handling is also studied.

This paper is organised as follows. Section 2 introduces the vehicle dynamics model that is applied by the controller. Then the optimal control problem is formulated in Section 3. In Section 4, the developed controller is validated in a Figure 8 scenario. Section 4.1 presents the simulation and testing results for validation of the controller. In Section 4.2, the effect of side slip angle reference in path-tracking control at the limits of handling is further studied and discussed. In Section 4.3, more testing are done with higher reference velocity which pushes the vehicle at the tyre's friction limits, so that the operation at the limits of handling can be confirmed.

2. Vehicle dynamics modelling

Figure 1(a) shows a picture of the testing vehicle for which the controller is developed in this paper, and Figure 1(b) shows the actuation topology of the specific vehicle. The vehicle in study is a 4WD EV prototype built by Delta Cosworth for the AID-CAV project. The powertrain includes three electric motors, responsible for both acceleration and deceleration of the vehicle. The motor M1 drives the front wheels through an open differential on the front axle, and the other two motors M2 and M3 drive the rear wheels respectively, which enables torque vectoring to be performed. In addition, the autonomous EV is equipped with 4WS functionality, which is realised by a steer-by-wire system. Despite that the control algorithm proposed here has been designed for the particular vehicle, it is extendable to fit most types of multi-actuation topology of EVs, including individual in-wheel hub motors.

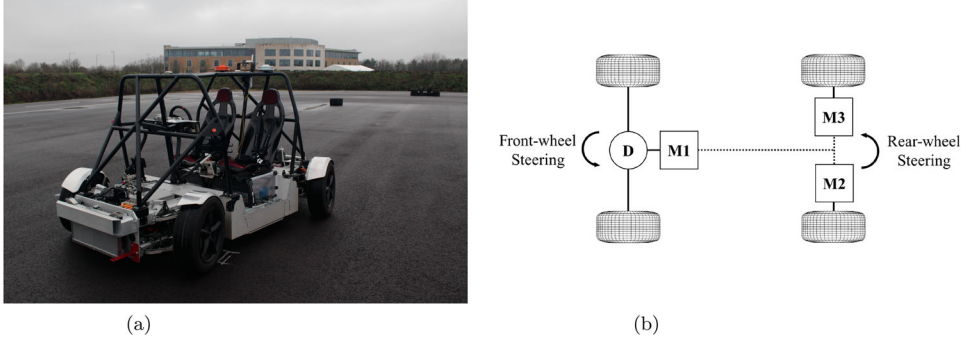

Figure 1. AID-CAV Phase 2B vehicle platform used as the testing vehicle. (a) Picture of the vehicle. (b) Actuator topology.

2.1. Equations of motion

The development of the proposed path-tracking controller is based on a double-track vehicle model formulated around the centre of gravity (CoG) of the vehicle. Under the assumption of horizontal motion, the vehicle's pitch, roll and heave motion can thus be neglected. The vehicle model is shown in Figure 2, and the equations of motion are given as follows:

$$\begin{aligned} m(\dot{V}_x - V_y r) &= (F_{FLx} + F_{FRx})\cos\delta_F - (F_{FLy} + F_{FRy})\sin\delta_F \\ &\quad + (F_{RLx} + F_{RRx})\cos\delta_R - (F_{RLy} + F_{RRy})\sin\delta_R \end{aligned} \tag{1}$$

$$\begin{aligned} m(\dot{V}_y + V_x r) &= (F_{FLx} + F_{FRx})\sin\delta_F + (F_{FLy} + F_{FRy})\cos\delta_F \\ &\quad + (F_{RLx} + F_{RRx})\sin\delta_R + (F_{RLy} + F_{RRy})\cos\delta_R \end{aligned} \tag{2}$$

$$\begin{aligned} I_z\dot{r} &= l_F \cdot (F_{FLx} + F_{FRx})\sin\delta_F + l_F \cdot (F_{FLy} + F_{FRy})\cos\delta_F \\ &\quad - l_R \cdot (F_{RLx} + F_{RRx})\sin\delta_R - l_R \cdot (F_{RLy} + F_{RRy})\cos\delta_R \\ &\quad - w_L \cdot (F_{FLx}\cos\delta_F - F_{FLy}\sin\delta_F) \\ &\quad - w_L \cdot (F_{RLx}\cos\delta_R - F_{RLy}\sin\delta_R) \\ &\quad + w_R \cdot (F_{FRx}\cos\delta_F - F_{FRy}\sin\delta_F) \\ &\quad + w_R \cdot (F_{RRx}\cos\delta_R - F_{RRy}\sin\delta_R), \end{aligned} \tag{3}$$

where m and I_z denote the vehicle's mass and moment of inertia about its vertical axis through CoG. l_F and l_R represent the distances from the front and rear axle to CoG, while

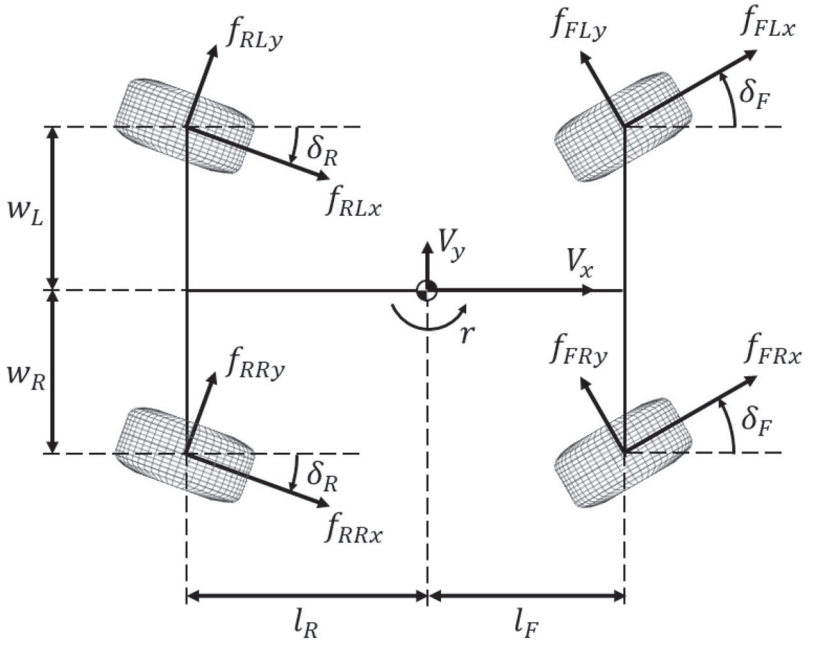

Figure 2. Schematic diagram of the vehicle model.

w_L and w_R refer to length of the left and right segments of the track width separated by CoG. The longitudinal and lateral velocity of the vehicle are denoted by V_x and V_y, and r refers to the yaw rate. F_{ijk} $(i = F, R,\ j = L, R,\ k = x, y)$ stands for the longitudinal and lateral tyre forces, while the steering angles on the front and rear wheels are denoted by δ_F and δ_R respectively.

For the path-tracking purpose, it is fundamental to include the vehicle position in the model. In this paper, the vehicle's position is expressed in the Cartesian coordinates, and the equations of motion for the vehicle position as well as yaw angle Ψ can be written as:

$$\dot{X} = V_x \cos(\Psi) - V_y \sin(\Psi) \tag{4}$$

$$\dot{Y} = V_x \sin(\Psi) + V_y \cos(\Psi) \tag{5}$$

$$\dot{\Psi} = r \tag{6}$$

2.2. Tyre model

When getting close to the limits of handling, the behaviour of vehicle dynamics becomes highly nonlinear due to the nonlinear characteristics of tyre force. As a result, in order to develop a controller for such kind of situation, it is necessary to apply an appropriate tyre model. Assuming that the pitch, roll and heave of the vehicle are neglected, the vertical load on wheels can be obtained based on the static weight distribution and the load transfer corresponding to the longitudinal and lateral acceleration. The vertical load on each wheel F_{ijz} is:

$$F_{FLz} = F_{FLz0} + \frac{mh}{lw} \cdot (-w_R a_x - l_R a_y) \tag{7}$$

$$F_{FRz} = F_{FRz0} + \frac{mh}{lw} \cdot (-w_L a_x + l_R a_y) \tag{8}$$

$$F_{RLz} = F_{RLz0} + \frac{mh}{lw} \cdot (w_R a_x - l_F a_y) \tag{9}$$

$$F_{RRz} = F_{RRz0} + \frac{mh}{lw} \cdot (w_L a_x + l_F a_y), \tag{10}$$

where a_x and a_y denote the vehicle's longitudinal and lateral acceleration respectively, and h stands for the distance from CoG to the ground. The static vertical force on each wheel of the vehicle is represented by F_{ijz0}.

Assuming that the turning radius is much larger than the wheelbase of the vehicle, small angles can be assumed, and thus the difference between inner and outer wheels can be negligible [33]. The side slip angles on the front and rear tyres can then be calculated by the following equations.

$$\alpha_F = \arctan \frac{V_y + l_F \cdot r}{V_x} - \delta_F \tag{11}$$

$$\alpha_R = \arctan \frac{V_y - l_R \cdot r}{V_x} - \delta_R \tag{12}$$

With the application of an appropriate constraint in the control formulation, it can be assumed that the tyre's adhesion limit is not exceeded in the longitudinal direction, and

hence the wheel rotational dynamics can be neglected [34]. With such assumption, the longitudinal tyre force is proportional to the torque applied on the wheels for driving or braking. In addition, since that the front wheels of the vehicle are driven by a single motor through an open differential, the torque on the front axle is assumed to be evenly delivered by the two front wheels. With T_F, T_{RL} and T_{RR} as the three control inputs, which stand for the torque on motor M1, M2 and M3 respectively, the longitudinal tyre force of the vehicle can be calculated as:

$$F_{Fjx} = \frac{T_F/2}{R_w} \tag{13}$$

$$F_{Rjx} = \frac{T_{Rj}}{R_w} \tag{14}$$

In the lateral direction, the tyre force on each wheel can be obtained through a simplified Pacejka's Magic Formula tyre model [35] as a function of the side slip angles on the tyres:

$$F_{ijy} = -F_{ijz} \cdot D \sin\left(C \arctan\left(B\alpha_i\right)\right) \tag{15}$$

In addition to the above 3DOF vehicle model, a bicycle model is used for the reference generation of the steering inputs. On the assumption of a much larger turning radius than the vehicle's wheelbase, the bicycle model can be obtained by representing left and right wheels with a single one, with a cornering force equivalent to both wheels.

Figure 3 shows a diagram of the bicycle model for reference generation. With the focus on lateral dynamics only, the EOM are given in the state space form by:

$$\begin{bmatrix} \dot{V}_y \\ \dot{r} \end{bmatrix} = \begin{bmatrix} -\frac{(C_F+C_R)}{mV_x} & -V_x - \frac{(l_FC_F-l_RC_R)}{mV_x} \\ -\frac{(l_FC_F-l_RC_R)}{I_zV_x} & -\frac{({l_F}^2C_F+{l_R}^2C_R)}{I_zV_x} \end{bmatrix} \cdot \begin{bmatrix} V_y \\ r \end{bmatrix} + \begin{bmatrix} \frac{C_F}{m} & \frac{C_R}{m} \\ \frac{l_FC_F}{I_z} & \frac{-l_RC_R}{I_z} \end{bmatrix} \cdot \begin{bmatrix} \delta_F \\ \delta_R \end{bmatrix}, \tag{16}$$

where C_F and C_R are the cornering stiffness of the front and rear tyres respectively.

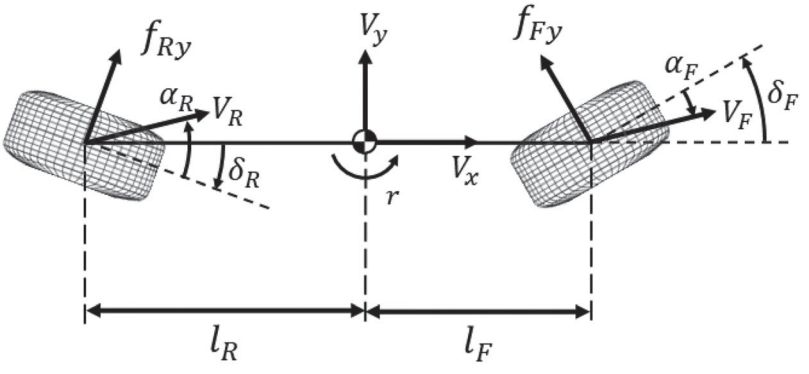

Figure 3. Bicycle model.

3. Predictive path-tracking controller

In this chapter, the controller is developed for the purpose of path tracking at the limits of handling with the application of MPC. The reference generation is first discussed in this chapter, following by the construction of the MPC optimisation problem.

In order to carry out path-tracking, a reference path is required for the controller. In this paper, the reference path is represented by the distance S from the origin point, where $S \in [0, L]$ and L refers to the full distance along the reference path. Taking advantage of some identified waypoints on the path, interpolation can be carried out for the parameterisation of the entire reference path [16]. Hence, the position $X_{ref}(S)$, $Y_{ref}(S)$ of any waypoint located on the path can be calculated through spline interpolation based on S as the argument. Additionally, the tangential angle of the reference path at a particular waypoint is used as the yaw angle reference for the controller, which can be calculated as

$$\Psi_{ref}(S) = \arctan \frac{\partial Y_{ref}(S)}{\partial X_{ref}(S)} \tag{17}$$

For path-tracking purpose, the relative position of the vehicle with regards to the reference path is required. Point $(X_{ref}(S_0), Y_{ref}(S_0))$ is proposed as the projection of the vehicle position on the reference path, and S_0 refers to the distance that the vehicle has travelled along the reference path. S_0 can be calculated through the following optimisation problem:

$$S_0 = \min_{S} \; [X - X_{ref}(S)]^2 + [Y - Y_{ref}(S)]^2 \tag{18}$$

Once S_0 is obtained, the distance between the projection point and the vehicle can be used to represent the lateral tracking error of the vehicle from the reference path.

For discrete-time control, a series of waypoints are required for reference generation. The waypoints are supposed to follow the projection point $(X_{ref}(S_0), Y_{ref}(S_0))$, with an interval of ΔS,

$$\Delta S = V_{ref} \cdot t_s, \tag{19}$$

where V_{ref} refers to the velocity reference and t_s stands for the sampling time of the controller. Figure 4 shows a diagram of the generated waypoints based on the vehicle's position and the velocity reference. The reference Cartesian coordinates and yaw angle are then calculated based on spline interpolation. In order to reduce computation time, only the reference path segment within a short horizon are included in the optimisation problem, and such horizon is proportional to the velocity of the vehicle. This helps to increase the efficiency of localisation while maintaining accurate solution on assumption that the vehicle does not deviate too much from the reference path.

The continuous-time system can be described as:

$$\dot{x}_t = f_c(x_t, \; u_t), \tag{20}$$

where x_t refers to the state vector $[V_x, V_y, r, X, Y, \Psi]^T$ and u_t stands for the control input vector $[\delta_F, \delta_R, T_F, T_{RL}, T_{RR}]^T$.

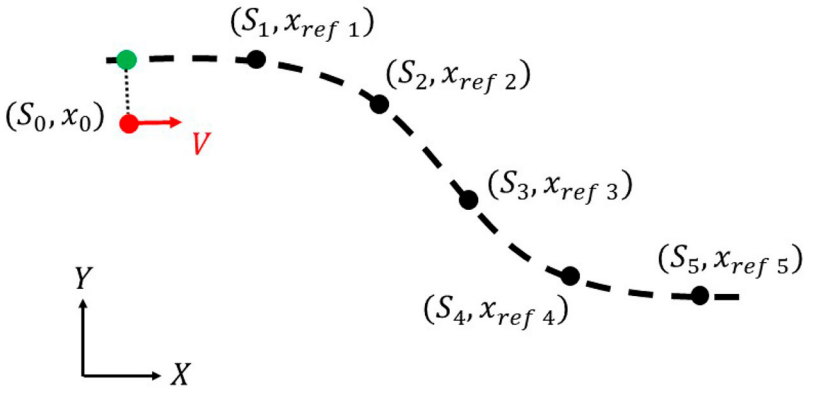

Figure 4. Diagram of waypoints on the reference path. The red dot stands for the vehicle's actual position, and its projection on the reference path is represented by the green dot. The waypoints have a fixed interval of $\Delta S = V_{ref} t_s$.

The main purpose of the controller is to follow the reference path at the reference velocity, and the discrete-time NMPC optimisation problem is formulated as

$$\begin{aligned}
&\min_{x,u} \sum_{k=0}^{N-1} (x_{k+1} - x_{ref,k+1})^T Q (x_{k+1} - x_{ref,k+1}) + (u_k - u_{ref,k})^T R (u_k - u_{ref,k}), \\
&\quad st.\ x_0 = x_{initial} \\
&\qquad x_{k+1} = f_d(x_k, u_k), \quad k = 0, 1, \ldots, N-1 \\
&\qquad x_{\min} \le x_k \le x_{\max}, \quad k = 0, 1, \ldots, N-1 \\
&\qquad u_{\min} \le u_k \le u_{\max}, \quad k = 0, 1, \ldots, N-1
\end{aligned} \tag{21}$$

where N is the prediction horizon steps, x_{ref} is the reference for state vector x, namely $[V_{x,ref}, V_{y,ref}, r_{ref}, X_{ref}, Y_{ref}, \Psi_{ref}]^T$, and Q, R are the weighting matrices for the states and control inputs respectively. f_d represents the discrete-time system of the model, which is obtained by applying explicit Runge-Kutta 4th order approach to discretise the continuous-time system f_c. While box constraints are used in this paper, they can easily be extended to include time-varying constraints on the control inputs if necessary.

The reference states are calculated with the bicycle model introduced in Chapter 2, according to the actual vehicle status.

By assuming a steady-state condition where $\dot{V}_y$ and $\dot{r}$ are zero, Equation (16) can be transformed as the following:

$$\begin{bmatrix} \delta_{F,SS} \\ \delta_{R,SS} \end{bmatrix} = -\begin{bmatrix} \frac{C_F}{m} & \frac{C_R}{m} \\ \frac{l_F C_F}{I_z} & \frac{-l_R C_R}{I_z} \end{bmatrix}^{-1} \cdot \begin{bmatrix} -\frac{(C_F + C_R)}{m V_{x,SS}} & -V_{x,SS} - \frac{(l_F C_F - l_R C_R)}{m V_{x,SS}} \\ -\frac{(l_F C_F - l_R C_R)}{I_z V_{x,SS}} & -\frac{(l_F^2 C_F + l_R^2 C_R)}{I_z V_{x,SS}} \end{bmatrix} \cdot \begin{bmatrix} V_{y,SS} \\ r_{SS} \end{bmatrix}, \tag{22}$$

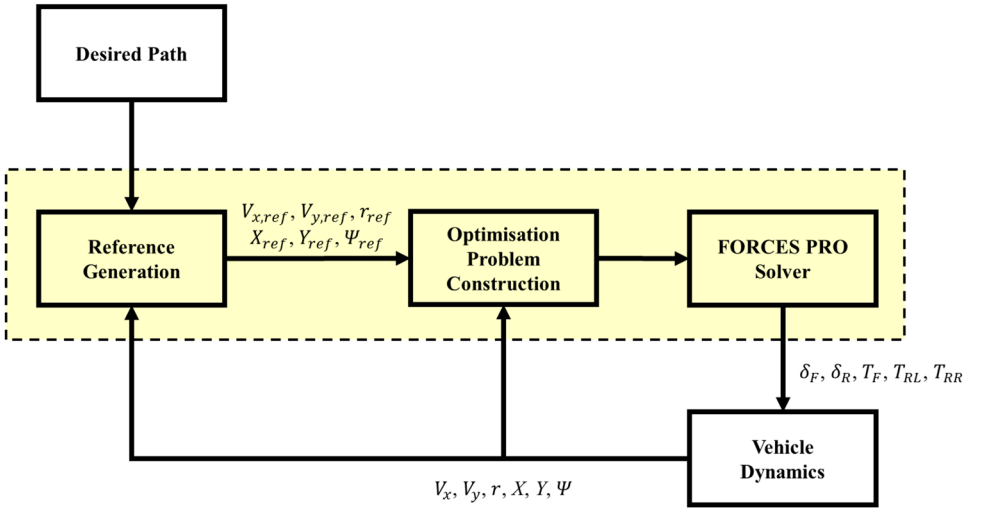

Figure 5. Diagram of the control system.

where $V_{x,SS}$, $V_{y,SS}$ and r_{SS} are the steady states of the vehicle according to the references, while $\delta_{F,SS}$ and $\delta_{R,SS}$ are the corresponding steering inputs. With Equation (22), references of the steering inputs can be calculated given the reference velocity, side slip angle and yaw rate. Providing such reference inputs to the controller helps to normalise the variation of steering actions during steady-state condition, and thus aids the stabilisation of the vehicle.

It is common in MPC control design, when constructing the cost function, penalties to be applied directly on the control inputs in order to minimise the control effort for purposes such as energy saving. However, minimal steering action is not expected in this research, as the vehicle is expected to be operating at the limits of handling condition. Hence, in addition to the target vehicle states including V_x, V_y, r as well as the position information, references of the steering inputs δ_F and δ_R are also provided to the controller.

Figure 5 shows the diagram of the complete control algorithm. The parameterisation of the desired path is completed offline prior to the simulation and testing. Within the controller, the references for the vehicle states are generated based on vehicle state feedback as well as the desired path. Then an optimisation problem is constructed as described in Equation (21). After the optimisation problem being solved by the NMPC solver, the control commands are transmitted to the lower level actuators to apply control on vehicle dynamics. The solver for the optimisation problem is generated using FORCES Pro [36,37].

4. Simulation and testing results

In this section, the path-tracking performance of the vehicle is validated in both simulation and testing. The simulation is carried out within IPG CarMaker, with a high fidelity vehicle model and scenario. Figure 8 path-tracking manoeuvre is used to validate the control performance, which is effective to evaluate the steady-state handling performance of the vehicle at its limits of handling. The introduction of a transient stage at the intersection of the two circles makes it a much more demanding manoeuvre. All the simulation sessions are run on a workstation laptop (Intel Core i7-8750H CPU at 2.2 GHz with 32GB RAM).

Table 1. System configuration of the controllers.

Parameter	Value	Parameter	Value
m (kg)	874.5	B (1)	9.50
I_z (kgm^2)	1597.7	C (1)	1.63
l (m)	1.995	D (1)	1.16
l_f (m)	0.815	C_F (1)	91393.39
l_r (m)	1.180	C_R (1)	63123.40
w (m)	1.530	$\delta_{F,lim}$ (deg)	19
w_l (m)	0.765	$\delta_{R,lim}$ (deg)	19
w_r (m)	0.765	$T_{F,lim}$ (Nm)	800
h (m)	0.297	$T_{R,lim}$ (Nm)	350

The testing sessions are run on a a real-time target machine Speedgoat Mobile (Intel Core i7-3555LE CPU at 2.5 GHz with 4GB RAM). During practical testing, the vehicle states required by the controller are measured by an OXTS RT1003, which is an inertial navigation system and applies real-time kinematic positioning as well as Kalman Filter to improve measurement accuracy to 0.0136 m for position, 0.0110 m/s for velocity and 0.0628 degrees for yaw angle.

Table 1 shows the parameters of the testing vehicle. A sampling time of 0.1 s and prediction horizon of 1 s are used for the NMPC algorithm. These are obtained by inspecting the control performance in simulation with various combination of sampling time and prediction horizon, and the particular combination provides relatively good performance while guaranteeing real-time operation.

4.1. Simulation and testing results for operation close to the limits of handling

As mentioned before, Figure 8 track is used as the reference path for the validation of the controller. It consists of two circles tangent to each other, and the radius of both circles are 8 m. A reference velocity of 8 m/s is given to the controller for the path-tracking purpose. In addition to that, two different side slip angle references are given. The vehicle tracks the reference path with 0° side slip angle reference first, and then with a 15° reference in the second run. It shall be pointed out that regarding limits of handling, this paper mainly focuses on lateral dynamics, but longitudinal control at the limits of handling can easily be established by replacing the constant velocity reference with a reference speed profile.

4.1.1. Figure fig8 tracking with 0° side slip angle reference

Figure 6 shows the vehicle states during the Figure 8 tracking with 0° side slip angle reference from both simulation and testing. Figure 6(a) shows the trajectory of the vehicle in comparison with the reference path, where the vehicle tracks the right circle in counterclockwise direction, followed by the left circle in clockwise direction. The g-g diagram is shown in 6(b), where the friction limit is calculated based on the peak factor of the tyre model. It suggests that the vehicle is operated quite close to its handling limit during this manoeuvre in the testing as well as simulation. According to Figure 6(c), the steady-state tracking error of the velocity is around 0.2 m/s in simulation, while more variation up to 0.5 m/s takes place in the experiment at the transient point, where the vehicle switches from one steady-state condition to another within 3 seconds. Figure 6(d) shows the side

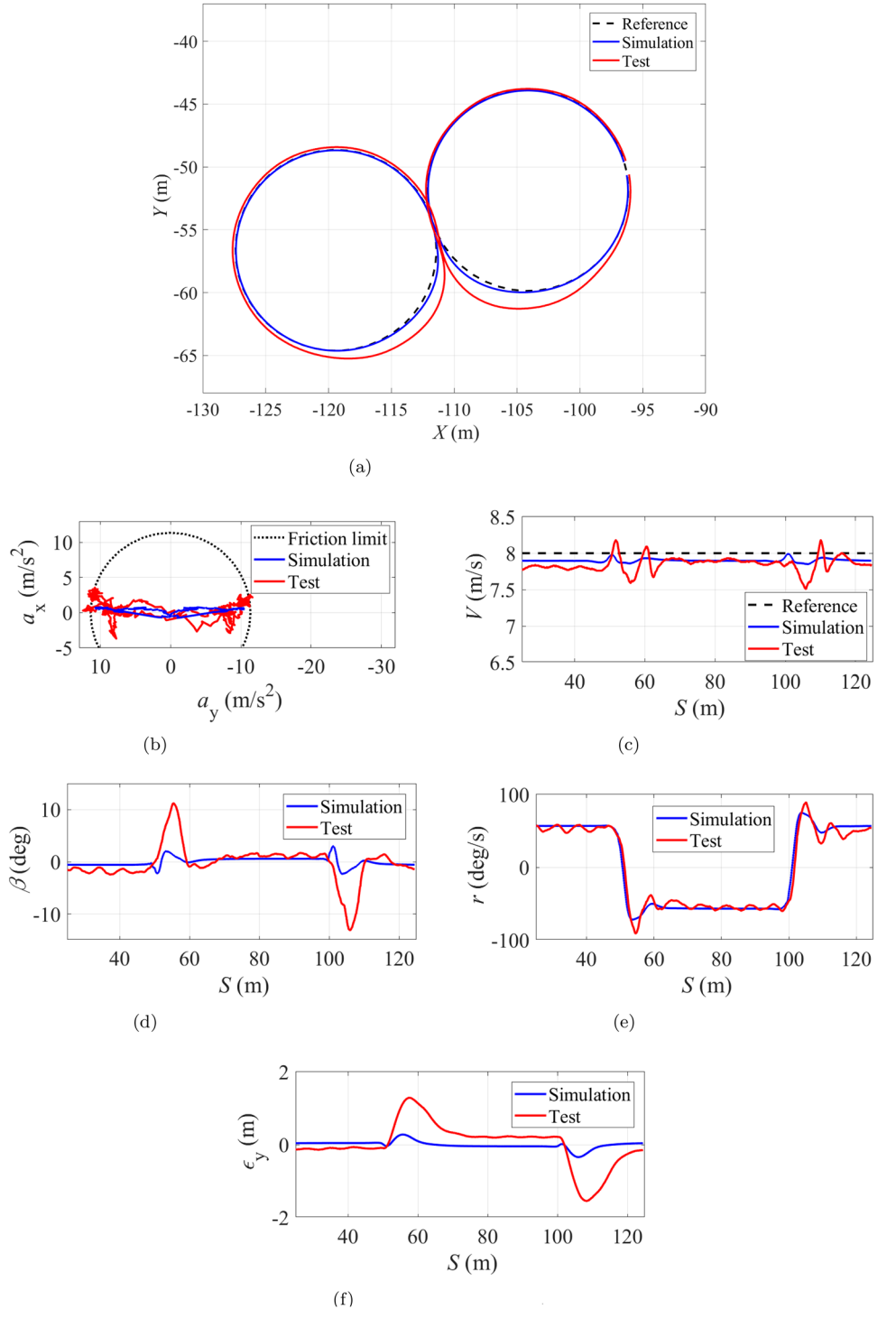

Figure 6. Vehicle states during Figure 8 tracking with 0° side slip angle reference. (a) Vehicle trajectory. (b) g-g diagram. (c) Velocity. (d) Side slip angle. (e) Yaw rate and (f) Lateral tracking error.

slip angle of the vehicle. The side slip angle of the vehicle remains relatively closer to zero in simulation especially during the steady-state condition, while spikes up to 12 degrees take place at the transient point in practical testing. The yaw rate of the vehicle is shown in Figure 6(e). Despite the oscillation in experiment data compared with simulation, the controller has done a good job in stabilising the vehicle in both simulation and testing under such an extreme condition. With the presence of the dramatic transition between two steady-state conditions, the controller has managed to stabilise the yaw rate efficiently. The lateral tracking error is shown in Figure 6(f). It can be seen that following the transient point, the vehicle deviated from the reference path due to the quick change of turning direction, and such deviation is larger in the testing. The controller is able to track Figure 8 path with a maximum deviation of 0.35 m in simulation, while the tracking error is up to 1.6 m in the experiment. The steady-state tracking error is around 0.2 m in practical testing, and is less than 0.05 m in simulation.

Figure 7 shows the control commands during the Figure 8 tracking. From Figure 7(a,b) it can be seen that opposite front and rear steering are applied by the controller during the steady-state turning. The front wheel torque command is shown in Figure 7(c). During transition, larger torque on the front wheels is required in order to compensate the loss in longitudinal velocity due to the harsh change in the lateral motion. Figure 7(d,e) shows the rear wheel torque commands. Differential torque on the rear axle can be observed in simulation which generates the yaw moment to stabilise the vehicle, and the difference is greater in the practical testing.

The computation time of the control system is shown in Figure 8. In simulation, the computation time is the time duration used by the FORCES Pro solver, while the computation time in testing refers to the total execution time of the real-time application running on Speedgoat. The controller takes about double the time in testing compared with simulation, while the computation time of both is below the 0.1 s sampling time boundary.

4.1.2. Figure fig8 tracking with 15° side slip angle reference

Following Figure 8 tracking with 0° side slip angle reference, a reference side slip angle of 15° is given to the controller, and the vehicle is still supposed to track Figure 8 path at a constant velocity of 8 m/s.

Figure 9 shows the vehicle states in simulation and experiment. It can be seen in Figure 9(a) that good tracking performance has been achieved by the controller in both simulation and experiments compared with 0° side slip angle reference, and the vehicle tends to cut the corner at the transition point to avoid going wide from the reference path. Figure 9(b) shows the acceleration of the vehicle, which confirms the operation of the vehicle close the limits of handling. As shown in Figure 9(c), variation in velocity takes place at the transition point, with the tracking error up to 0.2 m/s in simulation and up to 0.6 m/s in the testing. Figure 9(d) shows the side slip angle of the vehicle compared to the reference. The controller is able to track the side slip reference with a steady-state error of less than 2 degrees. Figure 9(e) shows the yaw rate of the vehicle, and it can be seen that the controller is effective in stabilising the vehicle in both simulation and experiment during the transition. In the practical testing, there is a larger overshoot in the yaw rate at the transition point, but the controller still manages to stabilise it in about 2 s. Figure 9(f) shows the lateral tracking error of the vehicle. The lateral deviation is maintained within 0.5 m in both simulation

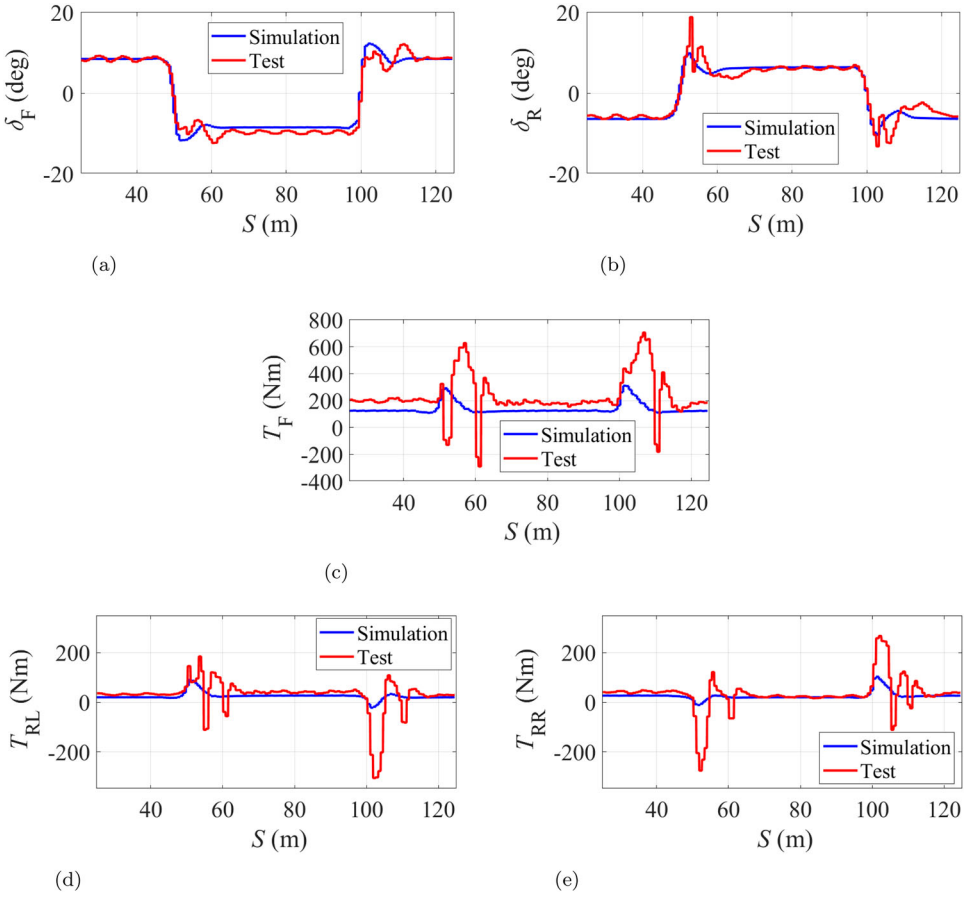

Figure 7. Control commands during Figure 8 tracking with 0° side slip angle reference. (a) Front steering commands. (b) Rear steering commands. (c) Front wheel torque commands. (d) Rear left wheel torque commands and (e) Rear right wheel torque commands.

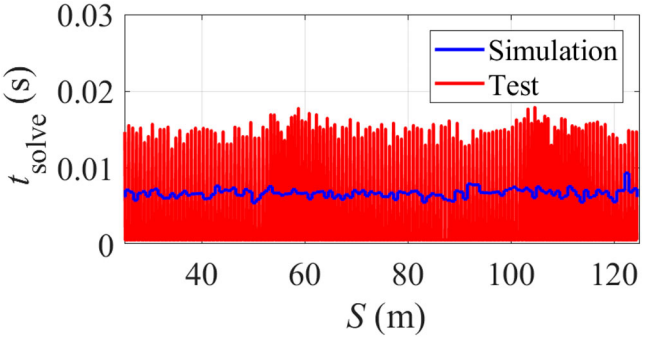

Figure 8. Computation time during Figure 8 tracking with 0° side slip angle reference.

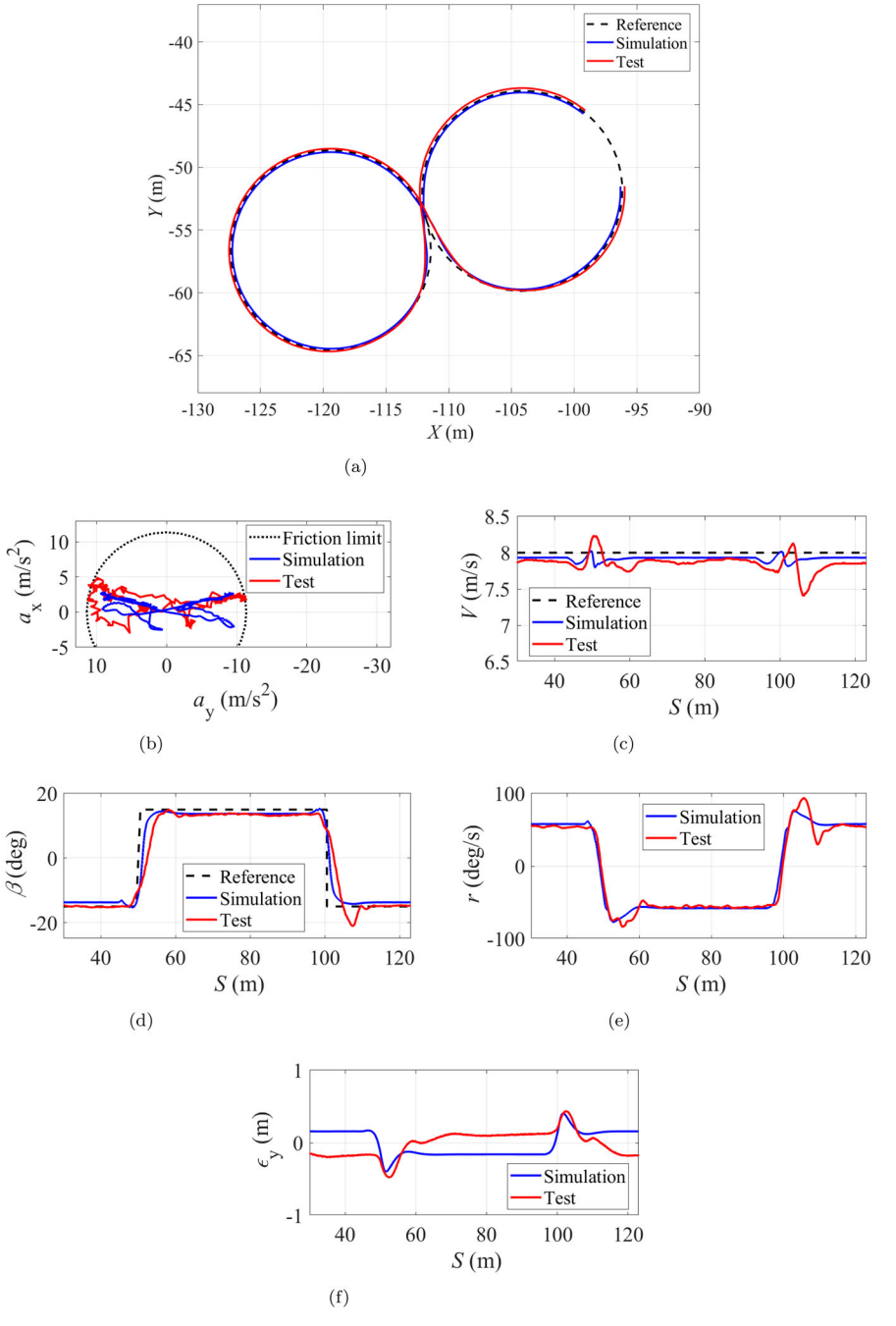

Figure 9. Vehicle states during Figure 8 tracking with 15° side slip angle reference. (a) Vehicle trajectory. (b) g-g diagram. (c) Velocity. (d) Side slip angle. (e) Yaw rate and (f) Lateral tracking error.

and testing, while the steady-state error is slightly larger than the Figure 8 tracking with 0° side slip angle reference. This is because the controller has to make a compromise in the cost function.

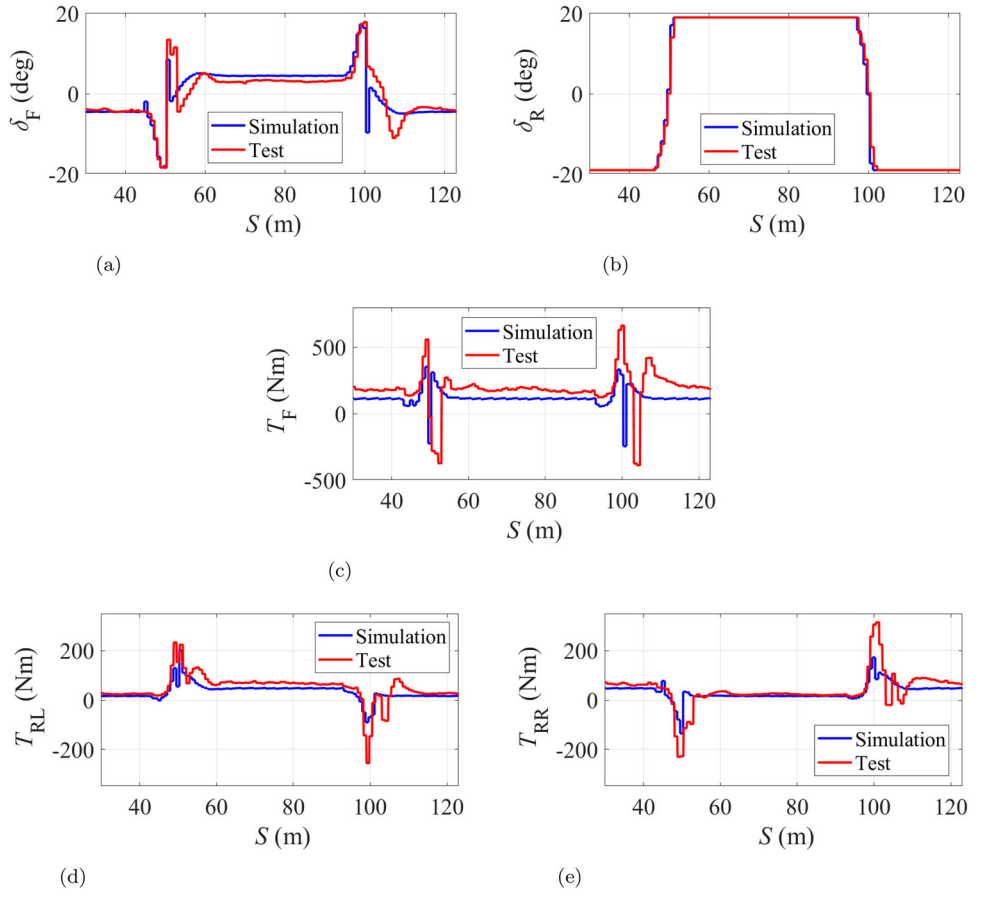

Figure 10. Control commands during Figure 8 tracking with 15° side slip angle reference. (a) Front steering commands. (b) Rear steering commands. (c) Front wheel torque commands. (d) Rear left wheel torque commands and (e) Rear right wheel torque commands.

Figure 10(a,b) shows the steering commands of the controller during operation. Different from the previous scenario, here the rear steering is saturated at its constraint of 19 degrees, while a smaller front steering angle in the same direction is demanded by the controller in both simulation and experiment. The front and rear steering in the same direction helps to track the side slip reference, and it is the difference between them that generates the required yaw moment for turning. By doing so, manipulating the vehicle's attitude such as side slip angle can be achieved. Figure 10(d,e) shows the rear wheel torque commands, and it can be seen that again large torque differential on the rear wheels takes place at the transition point to compensate the required yaw moment to change the direction of the vehicle promptly while maintaining vehicle stabilisation. The computation time of the control system is shown in Figure 11.

Figure 8 manoeuvre introduces a significant transition between steady-state conditions, which raises high requirements on the effectiveness and robustness of the controller. According to the results in both simulation and practical testing shown in this section, the proposed controller has shown its capability of stabilising autonomous vehicles during

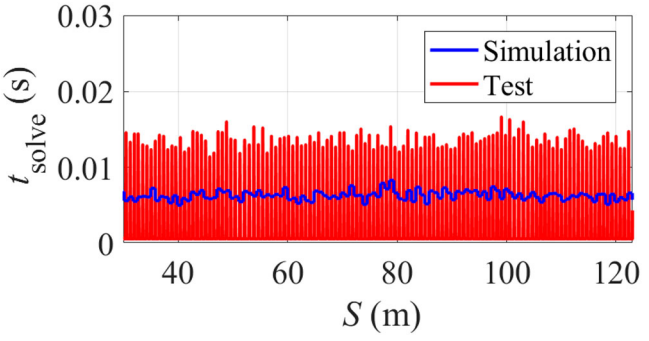

Figure 11. Computation time during Figure 8 tracking with 15° side slip angle reference.

extreme conditions. Moreover, Figure 8 tracking with side slip reference demonstrates the capability of the proposed controller in manipulating the vehicle's attitude relative to the reference path, which is done by providing a side slip angle reference to the vehicle.

4.2. Effect of side slip angle reference on path-tracking control performance

In Section 4.1, it is shown that the proposed controller is able to track different side slip angle reference at the limits of handling, while it also indicates that the side slip angle reference could have an influence on the performance of path-tracking control, which is further investigated in this section based on the testing results. Figure 12 shows the trajectories of the vehicle during testing when following reference velocity from 5 m/s to 9 m/s with side slip angle reference from 0° to 20°, and the RMS as well as max lateral tracking error under each condition are shown in Figure 13. First of all, a trend could be observed that when getting closer to the limits of handling, the vehicle deviates farther from the reference path. In addition, it can be seen that with a side slip angle reference of 0°, the vehicle has relatively the worst path-tracking performance in most of the conditions, which takes place after the transient point. This is because a 0° side slip angle reference would discourage the vehicle from promptly changing its turning direction, and this is especially affecting the path-tracking performance at the limits of handling condition. With a larger side slip angle reference, the lateral tracking error tends to be smaller, but this does not behave monotonically. From Figure 13, it could be seen that with a side slip angle reference of 15°, the vehicle tends to achieve a relatively smaller lateral tracking error, especially when the vehicle is close to the limits of handling. This demonstrates that an appropriate side slip angle reference plays a non-neglectable role in the path-tracking control at the limits of handling. A similar impact was also presented in Ref. [38], which carried out steady state analysis of a vehicle near the limits of handling. Despite being based on a rear-wheel-drive vehicle without TV, it was concluded that as the steady-state radius decreased, the maximum steady-state speed was achieved with an increased side slip angle. Further investigation is to be done on how the appropriate side slip angle reference can be obtained for tracking an arbitrary path with the control algorithm proposed in this work.

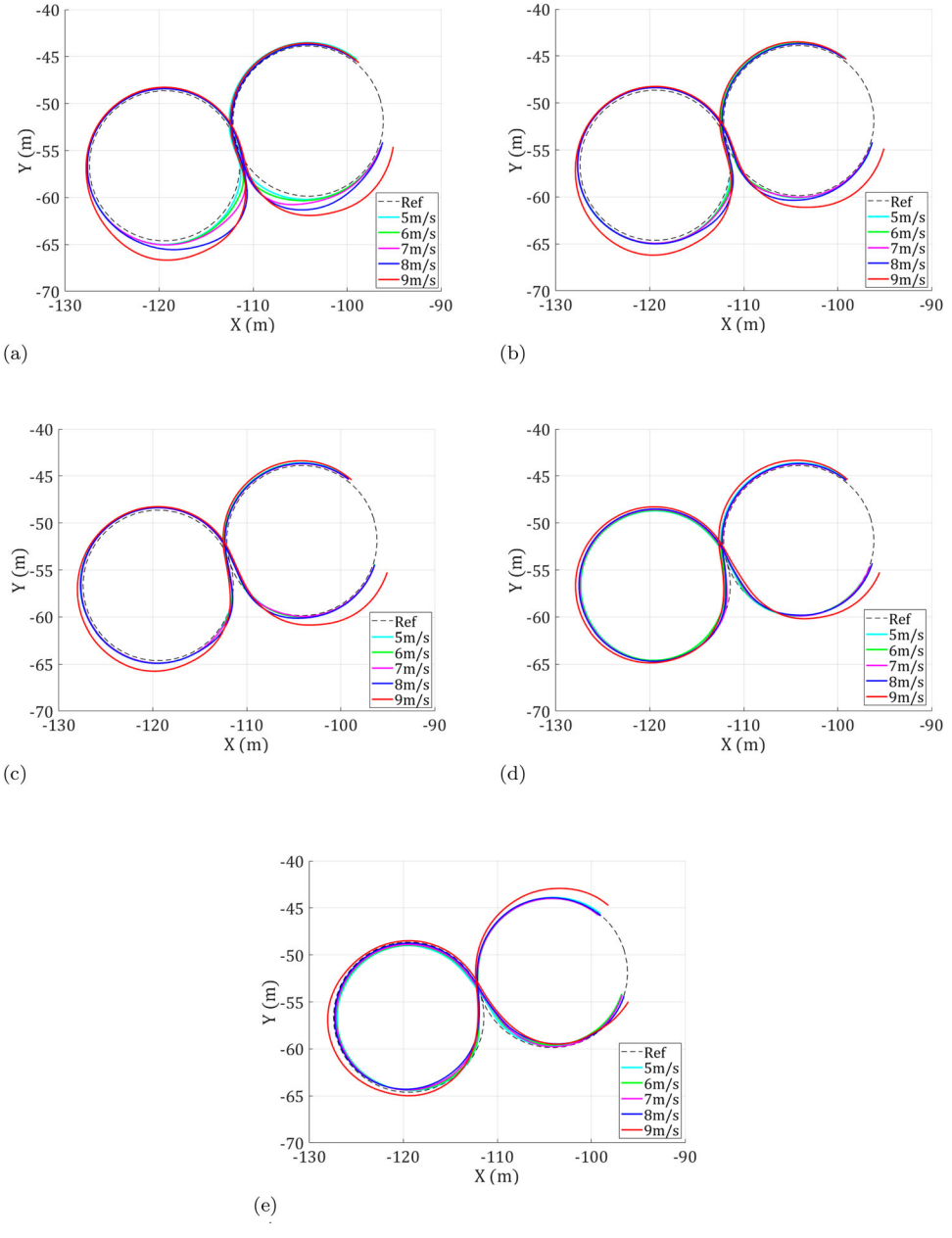

Figure 12. Vehicle trajectories during Figure 8 at various reference velocity with different side slip angle reference. (a) Vehicle trajectories at various reference velocity with 0° side slip angle reference. (b) Vehicle trajectories at various reference velocity with 5° side slip angle reference. (c) Vehicle trajectories at various reference velocity with 10° side slip angle reference. (d) Vehicle trajectories at various reference velocity with 15° side slip angle reference and (e) Vehicle trajectories at various reference velocity with 20° side slip angle reference.

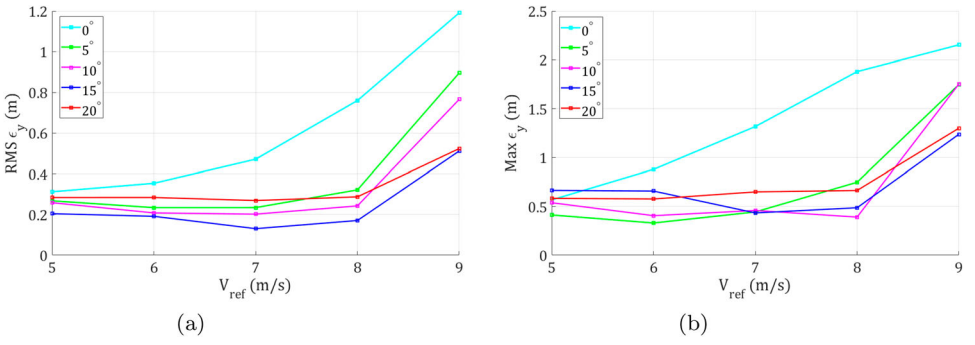

Figure 13. Lateral tracking error at various reference velocity with different side slip angle reference. (a) RMS error. (b) Max error.

4.3. *Vehicle operation at the limits of handling*

Further experiments have been conducted during vehicle testing to prove that the vehicle is operating at the limits of handling. In order to do so, reference velocity beyond 9 m/s has been given until 10.5 m/s with an increment of 0.5 m/s. Figure 14 shows the vehicle trajectories with different reference velocity, and Figure 15 shows the total acceleration of the vehicle in these conditions. It can be seen that compared with 8 m/s reference velocity, the vehicle is closer to the limits of handling at 9 m/s, while the acceleration retains around the friction limits beyond 9 m/s reference velocity. As shown in 14, with the increase of

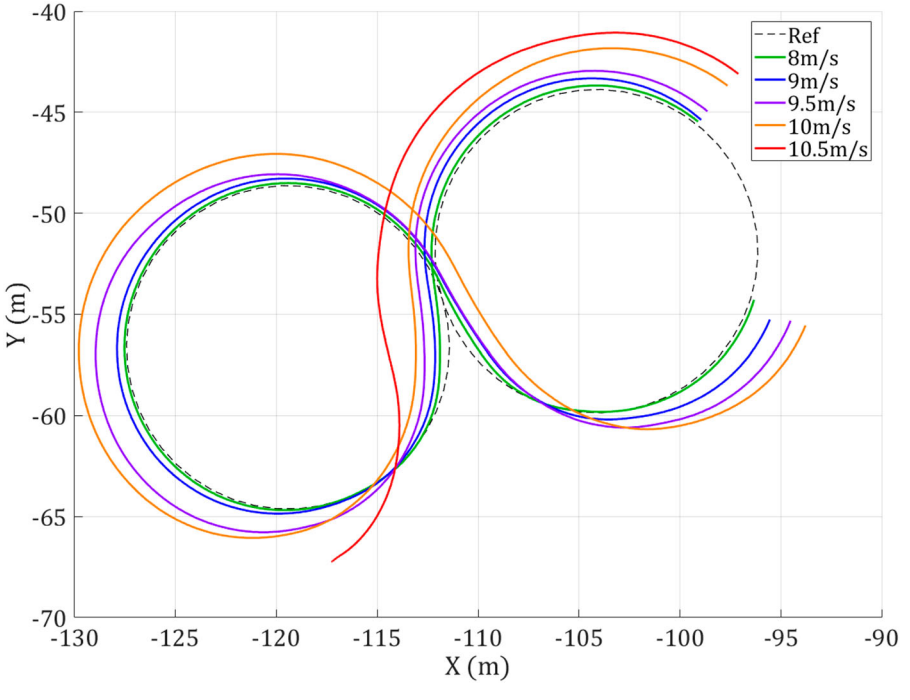

Figure 14. Vehicle trajectories close to the limits of handling with 15 degrees of side slip angle.

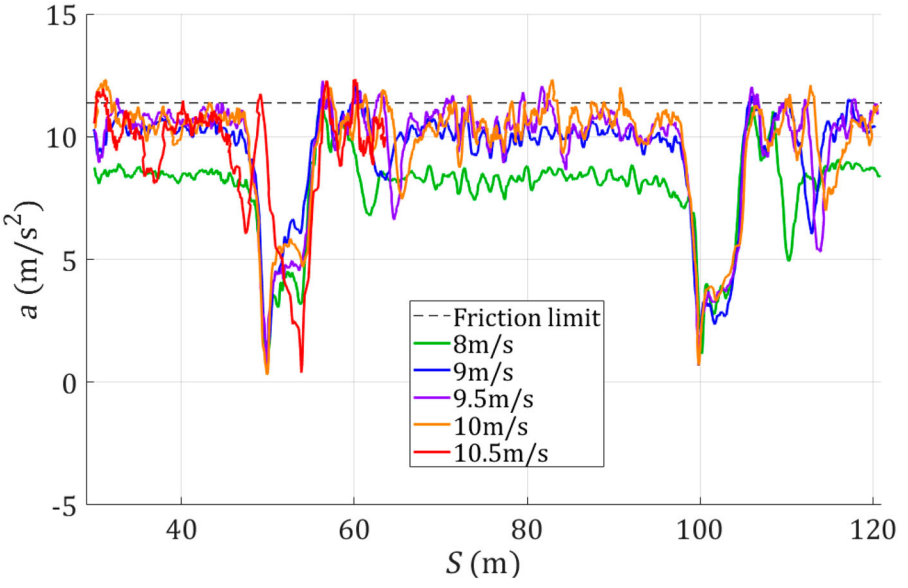

Figure 15. Vehicle acceleration with 15° side slip angle reference.

Table 2. Velocity tracking error at the limits of handling.

V_{ref} [m/s]	RMS Error [m/s]	Max Error [m/s]
8.0	0.184	0.59
9.0	0.285	0.68
9.5	0.437	1.17
10.0	0.759	1.82

reference velocity, the vehicle deviates from the reference path further and further. This is because since the vehicle is already at the limits of handling, higher reference velocity could only be achieved by enlarging the turning radius, at the cost of worse path-tracking performance. The RMS and max velocity tracking error under different reference velocity are shown in Table 2. It should be noticed that the vehicle loses control at the run of 10.5 m/s, which also indicates that the vehicle is operating at the limits of handling before it reaches instability.

5. Conclusion

In this paper, a controller is developed for an over-actuated electric vehicle. The controller is capable of path-tracking at the limits of handling, by exploiting the full vehicle dynamical capability with 4WS and TV functionalities. The control design is based on NMPC, and the system dynamics for MPC formulation is based on a 3DOF vehicle model taking into account the non-linearities in vehicle dynamics and tyre force, which is critical for vehicle control at the limits of handling. The MPC controller is formulated based on this vehicle model, together with the vehicle state reference generated according to a simplified bicycle model. The basic idea of the controller is to maintain the vehicle states as close to the reference as possible, while respecting the constraints in the actuation.

The proposed controller is validated in both simulation and practical testing. The controller is tested in Figure 8 scenario, which includes a significant transition between steady conditions and thus is a challenge for the controller to stabilise the vehicle especially at the limits of handling. The results of both simulation and testing show that the proposed controller is able to carry out path-tracking and stability control at the limits of handling. The proposed controller is capable of tracking the reference trajectory while maintaining the vehicle stability, which demonstrates its robustness. In addition to that, it is also able to manipulate the attitude of the vehicle when a side slip angle reference is provided.

The vehicle is then tested with different side slip angle reference to investigate its influence on the path-tracking control performance. With a reference side slip angle of 15°, the vehicle is able to track the reference path with relatively the smallest deviation. This demonstrates that side slip angle reference plays an important role in path-tracking control at the limits of handling. Future work will be carried out regarding the identification of the optimal side slip angle reference for different conditions.

Finally, the vehicle is pushed beyond its friction limit with higher reference velocity until it loses control. It is confirmed that the vehicle is operating at the limits of handling at around 9 m/s, and the proposed controller is still able to carry out path-tracking stabilisation with a relatively small deviation.

In summary, the control algorithm developed in this paper has been proven effective in enhancing the vehicle stability as well as performance at the limits of handling. It makes use of 4WS and TV to maximise the dynamical capability and flexibility of the vehicle. Furthermore, the controller is real-time implementable and has been validated in practical testing. The controller has shown itself widely suitable for different scenarios and control objectives, with consistent control performance and robustness. This would be useful for application such as enhancing road performance of autonomous vehicles, and stability control in emergency conditions.

In future work, the sensitivity of the proposed controller to parameter variation is to be studied. In addition, a steady-state analysis will be performed for the proposed control topology, to further investigate how the side slip angle reference affects the path-tracking performance at the limit handling condition, and to work out an approach for identifying the appropriate side slip angle reference for tracking an arbitrary path.

Acknowledgments

The authors confirm that the data supporting this study are included within the article.

Disclosure statement

No potential conflict of interest was reported by the author(s).

Funding

This work is supported by Innovate UK under the AID-CAV project (project reference 104277).

References

[1] Katrakazas C, Quddus M, Chen W, et al. Real-time motion planning methods for autonomous on-road driving: state-of-the-art and future research directions. Transp Res Part C Emerg Technol. 2015;60:416–442. doi: 10.1016/j.trc.2015.09.011

[2] Schwesinger U, Rufli M, Furgale P, et al. A sampling-based partial motion planning framework for system-compliant navigation along a reference path. In: 2013 IEEE Intelligent Vehicles Symposium (IV); 2013. p. 391–396.

[3] Bonab SA, Emadi A. Optimization-based path planning for an autonomous vehicle in a racing track. In: IECON 2019 – 45th Annual Conference of the IEEE Industrial Electronics Society; Vol. 1; 2019. p. 3823–3828.

[4] Faulwasser T, Kern B, Findeisen R. Model predictive path-following for constrained nonlinear systems. In: Proceedings of the 48h IEEE Conference on Decision and Control (CDC) held jointly with 2009 28th Chinese Control Conference; 2009. p. 8642–8647.

[5] Laurense VA, Goh JY, Gerdes JC. Path-tracking for autonomous vehicles at the limit of friction. In: 2017 American Control Conference (ACC); 2017. p. 5586–5591.

[6] Madås D, Nosratinia M, Keshavarz M, et al. On path planning methods for automotive collision avoidance. In: 2013 IEEE Intelligent Vehicles Symposium (IV); 2013. p. 931–937.

[7] Funke J, Brown M, Erlien SM, et al. Collision avoidance and stabilization for autonomous vehicles in emergency scenarios. IEEE Trans Control Syst Technol. 2017;25(4):1204–1216. doi: 10.1109/TCST.2016.2599783

[8] Coulter RC. Implementation of the pure pursuit path tracking algorithm. Pittsburgh (PA): Carnegie Mellon University; 1991. CMU-RI-TR-92-01.

[9] Hoffmann GM, Tomlin CJ, Montemerlo M, et al. Autonomous automobile trajectory tracking for off-road driving: controller design, experimental validation and racing. In: 2007 American Control Conference; 2007. p. 2296–2301.

[10] Roselli F, Corno M, Savaresi SM, et al. H∞ control with look-ahead for lane keeping in autonomous vehicles. In: 2017 IEEE Conference on Control Technology and Applications (CCTA); 2017. p. 2220–2225.

[11] Tagne G, Talj R, Charara A. Higher-order sliding mode control for lateral dynamics of autonomous vehicles, with experimental validation. In: 2013 IEEE Intelligent Vehicles Symposium (IV); 2013. p. 678–683.

[12] Lee K, Jeon S, Kim H, et al. Optimal path tracking control of autonomous vehicle: adaptive full-state linear quadratic Gaussian (LQG) control. IEEE Access. 2019;7:109120–109133. doi: 10.1109/Access.6287639

[13] Vivek K, Sheta MA, Gumtapure V. A comparative study of Stanley, LQR and MPC controllers for path tracking application (ADAS/AD). In: 2019 IEEE International Conference on Intelligent Systems and Green Technology (ICISGT); 2019. p. 67–71.

[14] Yakub F, Mori Y. Comparative study of autonomous path-following vehicle control via model predictive control and linear quadratic control. Proc Inst Mech Eng Pt D J Automobile Eng. 2015;229(12):1695–1714. doi: 10.1177/0954407014566031

[15] Alessandretti A, Aguiar AP, Jones CN. Trajectory-tracking and path-following controllers for constrained underactuated vehicles using model predictive control. In: 2013 European Control Conference (ECC); 2013. p. 1371–1376.

[16] Liniger A, Domahidi A, Morari M. Optimization-based autonomous racing of 1:43 scale RC cars. Optim Control Appl Methods. 2015;36(5):628–647. doi: 10.1002/oca.v36.5

[17] Dai C, Zong C, Chen G. Path tracking control based on model predictive control with adaptive preview characteristics and speed-assisted constraint. IEEE Access. 2020;8:184697–184709. doi: 10.1109/Access.6287639

[18] Awad N, Lasheen A, Elnaggar M, et al. Model predictive control with fuzzy logic switching for path tracking of autonomous vehicles. ISA Trans. 2022;129:193–205. doi: 10.1016/j.isatra.2021.12.022

[19] Chatzikomis C, Sorniotti A, Gruber P, et al. Comparison of path tracking and torque-vectoring controllers for autonomous electric vehicles. IEEE Trans Intell Veh. 2018;3(4):559–570. doi: 10.1109/TIV.2018.2874529

[20] Siampis E, Velenis E, Longo S. Model predictive torque vectoring control for electric vehicles near the limits of handling. In: 2015 European Control Conference (ECC); 2015. p. 2553–2558.
[21] Vasiljevic G, Bogdan S. Model predictive control based torque vectoring algorithm for electric car with independent drives. In: 2016 24th Mediterranean Conference on Control and Automation (MED); 2016. p. 316–321.
[22] Mikuláš E, Gulan M, Takács G. Model predictive torque vectoring control for a formula student electric racing car. In: 2018 European Control Conference (ECC); 2018. p. 581–588.
[23] Guo J, Luo Y, Li K, et al. Coordinated path-following and direct yaw-moment control of autonomous electric vehicles with sideslip angle estimation. Mech Syst Signal Process. 2018;105:183–199. doi: 10.1016/j.ymssp.2017.12.018
[24] Chen T, Chen L, Xu X, et al. Simultaneous path following and lateral stability control of 4wd-4ws autonomous electric vehicles with actuator saturation. Adv Eng Softw. 2019;128:46–54. doi: 10.1016/j.advengsoft.2018.07.004
[25] Acosta M, Kanarachos S, Fitzpatrick ME. On full magv lateral dynamics exploitation: autonomous drift control. In: 2018 IEEE 15th International Workshop on Advanced Motion Control (AMC); 2018. p. 529–534.
[26] Kapania NR, Gerdes JC. Design of a feedback-feedforward steering controller for accurate path tracking and stability at the limits of handling. Veh Syst Dyn. 2015;53(12):1687–1704. doi: 10.1080/00423114.2015.1055279
[27] Torres EM, Martinez CO, Bianchi FD. Experimental modelling and optimal torque vectoring control for 4wd vehicles. IEEE Trans Veh Technol. 2022;71(5):4922–4932. doi: 10.1109/TVT.2022.3158091
[28] Barari A, Afshari SS, Liang X. Coordinated control for path-following of an autonomous four in-wheel motor drive electric vehicle. Proc Inst Mech Eng Pt C: J Mech Eng Sci. 2022;236(11):6335–6346. doi: 10.1177/09544062211064797
[29] Hiraoka T, Nishihara O, Kumamoto H. Automatic path-tracking controller of a four-wheel steering vehicle. Veh Syst Dyn. 2009;47(10):1205–1227. doi: 10.1080/00423110802545919
[30] Ren Y, Zheng L, Khajepour A. Integrated model predictive and torque vectoring control for path tracking of 4-wheel-driven autonomous vehicles. IET Intell Transp Syst. 2019;13(1):98–107. doi: 10.1049/itr2.v13.1
[31] Jeong Y, Yim S. Path tracking control with four-wheel independent steering, driving and braking systems for autonomous electric vehicles. IEEE Access. 2022;10:74733–74746. doi: 10.1109/ACCESS.2022.3190955
[32] Lin C, Siampis E, Velenis E. Real-time path-tracking mpc for an over-actuated autonomous electric vehicle. In: 2022 American Control Conference (ACC); 2022. p. 2006–2011.
[33] Gillespie TD. Fundamentals of vehicle dynamics. Warrendale (PA): Society of Automotive Engineers; 1992.
[34] Zarkadis K, Velenis E, Siampis E, et al. Predictive torque vectoring control with active trail-braking. In: 2018 European Control Conference (ECC); 2018. p. 569–574.
[35] Pacejka HB, Bakker E. The magic formula tyre model. Veh Syst Dyn. 1992;21(sup001):1–18. doi: 10.1080/00423119208969994
[36] Domahidi A, Jerez J. Forces professional [Embotech ag. Available from: https://embotech.com/forces-pro]; 2014–2019.
[37] Zanelli A, Domahidi A, Jerez J, et al. Forces nlp: an efficient implementation of interior-point methods for multistage nonlinear nonconvex programs. Int J Control. 2017;93(1):13–29. doi: 10.1080/00207179.2017.1316017
[38] Velenis E, Katzourakis D, Frazzoli E, et al. Steady-state drifting stabilization of rwd vehicles. Control Eng Pract. 2011;19(11):1363–1376. doi: 10.1016/j.conengprac.2011.07.010

Path-tracking control at the limits of handling of a prototype over-actuated autonomous vehicle

Lin, Chenhui

2024-05-31

Lin C, Siampis E, Velenis E. (2024) Path-tracking control at the limits of handling of a prototype over-actuated autonomous vehicle. Vehicle System Dynamics, Available online 31 May 2024
https://doi.org/10.1080/00423114.2024.2361726